Propagation of ionizing electron shock waves in electrical breakdown

P. Bayle and B. Cornebois
Laboratoire de Génie Electrique, Université Paul Sabatier, 31062 Toulouse Cédex, France
(Received 6 April 1984; revised manuscript received 17 July 1984)

A numerical solution of a hydrodynamic second-order model shows that the propagation of the first ionizing wave arises from an overgrowth of hot electrons in the wave front in a zone of a greatly disturbed electric field. This gives rise, in the electron shock zone ahead of the wave, to a precursor phenomenon, whose effect is to accelerate the channel propagation. Inside the shock zone, the electronic energy differs from the characteristic energy; the nonequilibrium between the electrons and the electric field, as a result of the electron pressure gradient, induces a heating of electrons in this zone. The space-charge electric field is calculated assuming that the discharge evolves in a variable ellipsoidal envelope with revolution symmetry around the propagation axis. The electron shock-wave structure is shown to maintain itself and to propagate during the evolution of the discharge. The results obtained from this second-order model are compared to those obtained from a classical first-order model in which the electron temperature is a function of the reduced electric field alone. This comparison allows us to define the concept of electron nonequilibrium in an electron shock wave and to show that it is the source of the high-speed propagation of the streamer. The close agreement of the results obtained from the second-order model with the experimental data justifies the formulation of the model, particularly that of the interaction operators of the energy equation.

I. INTRODUCTION

The inception of breakdown in a gas, i.e., the phenomenon of a gas changing from an insulating state to a conducting state, is determined by a succession of ionizing waves reflected one after another on the electrodes, which gradually increases the ionization degree of the gas. This transition from the insulating state to the conducting state is well known to be controlled by the formation and the propagation of the first ionizing wave, giving rise to the ionized path through which the following waves propagate. Although this first ionizing wave has been studied experimentally by the most sophisticated diagnostic methods (such as high-speed image converter techniques), the mechanisms leading to its propagation in the neutral gas must be clarified in a fundamental way, particularly in the high-speed stage of the propagation, as the classic concept of Townsend avalanche no longer explains this propagation.

Many theoretical works try to explain this propagation process. Most of them are based on a hydrodynamic formulation of the ionized gas. Two different models have been used. The first-order models are only based on continuity equations for electron and ion densities. Electrons are supposed to be in equilibrium with the electric field, and the macroscopic coefficients used in the equations are experimental data obtained in the case of stationary or slightly transitory experimental discharges. All these models are one-dimensional but the discharge pattern is taken into account through a three-dimensional electric field calculation dealing with the radial expansion of the discharge. Davies, Davies, and Evans,[1] Kline,[2] Yoshida, and Tagashira,[3] and Bayle and Bayle[4] have shown the importance of the electric field perturbation, due to the space-charge effect, in the multiplication process and in the propagation of the electron swarm, in the case of electronegative as well as nonelectronegative gases. Abbas and Bayle[5] have shown the limits of validity of these first-order models for the study of the propagation of the first ionizing wave. They showed that the structure of this first ionizing wave always evolves towards an electron shock-wave structure and the large gradients of the electric field and densities no longer allow consideration of the electrons in equilibrium with the field, and so the classic macroscopic coefficients concept is no longer valid. In fact, there is no direct relation between the electric field and the electron temperature. This implies that the multiplication processes are explicit functions of the local electron temperature, which depends not only on the reduced electric field but also on the collective phenomena of the discharge. Thus it becomes necessary to develop second-order models taking into account the electron shock-wave structure of the wave and allowing the local-electron-temperature calculation, which is the most important point of the ionizing wave propagation.

Fowler and his students[6,7] used a multifluid hydrodynamic model to describe the ionizing wave in a stationary state. This stationary condition is characterized by a zero total current (electronic plus ionic). The description of the ionizing wave is obtained by two solutions. One of them, which is continuous, is representative of the antiforce waves and the other discontinuous solution is the solution of the proforce waves. The ionizing wave is then characterized by a discontinuity of its front where the electric field and the electron temperature reach their higher values. They assumed that the electron pressure gradient was the force governing the wave. It is thus possible to set up an analytic approach expression for the

wave speed versus this electron-temperature value.

Albright and Tidmann[8] studied the transitory wave propagation with a strong electric field. They used a hydrodynamic time-dependent model for the electronic densities, the electric field being linked only to the electron variables. In the case of the proforce waves, the electric field gives rise to the electron drift whereas for the antiforce waves, the electron pressure gradient reinforced by the electric field is the real propagation force. Klingbeil, Tidmann, and Fernsler[9] tried to take into account the role of photoionization with a time-dependent equivalent model. They obtained stationary solutions for the positive and negative waves. Abbas and Bayle[10] put forth a hydrodynamic model to define and analyze the structure of an electron shock wave when the electrons are no longer in equilibrium with the electric field. They pointed out that photoionization plays no role in the propagation as long as the nitrogen pressure is more than 50 Torr. They particularly studied the reasons of nonequilibrium between the electrons and the electric field and its possible effects on the electron diffusion and on the plasma source term, both these processes being essentially functions of the electron temperature. They showed that the structure of the wave is necessarily dynamic and that a permanence of the shock profile exists.

Jurenka and Barreto[11] studied the different terms for the energy gains and losses and compared their relative magnitude. They concluded that the electron fluid wave is driven by electron pressure gradients in weakly ionized plasmas. At the same time, the experimental results obtained by Jurenka[12] supported the concept of wave propagation through the collision-dominated electrons.

In this work, we concentrate on the study of the electron shock-wave propagation, the geometric and electric properties of the front of the discharge being particularly defined. The second-order hydrodynamic model put forth earlier by Abbas and Bayle[10] is improved, modifying the one-dimensional behavior of the hydrodynamic model by a three-dimensional calculation of the electric field. As the lines of force of the electric field are modified by the space-charge field, the discharge always evolves in a filamentary way, and this confining of the lines of force is taken into account in defining the profile of the front of the discharge. We assume that the discharge is enclosed in an ellipsoidal envelope with revolution symmetry around the direction of propagation of the discharge. The permanence of the electron shock-wave structure, appearing at the ellipsoidal envelope tip, is studied. The electron shock-wave results in a heating of the electrons ahead of the front and these electrons grow in number and speed up the propagation of the entire discharge. The high-speed propagation of the so-called streamer is the result of the superimposition of the effects of transport in a strong electric field and of the effects of overgrowth of hot electrons appearing in the electron shock-wave area.

II. DESCRIPTION OF THE HYDRODYNAMIC MODEL FOR NONEQUILIBRIUM TRANSITORY DISCHARGES

A. Dynamics of an electron fluid

This model rests on the equations of the hydrodynamics of weakly ionized gases governing the mean values of the fundamental parameters of the discharge state (charge-carrier densities, speed, energy, etc.). This set of equations is directly deduced from Boltzmann equation giving the behavior of the distribution function $f(\vec{r},w,\vec{t})$

$$\frac{\partial f}{\partial t}+\vec{w}\cdot\vec{\nabla}_r f+\frac{\vec{F}}{m}\cdot\vec{\nabla}_w f=\left[\frac{\partial f}{\partial t}\right]_{\text{int}}, \tag{1}$$

where $\vec{r},\vec{w}$ are the position and velocity for the particles, $(\partial f/\partial t)_{\text{int}}$ is the interaction term between the particles, $\vec{F}$ is the external force acting on the particles, and m is the mass of the particles.

If j represents one of the components of the gas (electrons, positive ions, negative ions, neutral particles, etc.) the equations for the three moments of Boltzmann equation are written, respectively, as

$$\frac{\partial n_j}{\partial t}+\vec{\nabla}_r(n_j\vec{v}_j)=S_{j\infty} \tag{2}$$

for the transport equation of density n_j for particle j, where

$$S_{j\infty}=\int\left[\frac{\partial f}{\partial E}\right]_{\text{int}}\underline{dw}_j$$

is the source term for particle j,

$$\frac{\partial(n_j m_j\vec{v}_j)}{\partial t}+\nabla_r(n_j m_j\vec{v}_j\cdot\vec{v}_j)+\vec{\nabla}_j\vec{\vec{P}}_j-n_j\vec{F}=R_1 \tag{3}$$

is the momentum transport equation, where

$$\vec{v}_j=\langle\vec{w}_j\rangle=\frac{1}{n_j}\int\vec{w}_j f\,\underline{dw}_j$$

is the mean speed of the particles j, where $\underline{dw}_j$ is the volume element in the velocity space $\underline{dw}_j=dw_{jx}dw_{jy}dw_{jz}$

$$\vec{\vec{P}}_j=n_j m_j(\vec{w}_j-\vec{v}_j)(\vec{w}_j-\vec{v}_j)$$

is the kinetic pressure tensor, and

$$R_1=\int m\vec{w}_j\left[\frac{\partial f}{\partial t}\right]_{\text{int}}\underline{dw}_j,$$

and

$$\frac{\partial}{\partial t}[n_j(\epsilon_j+\tfrac{1}{2}m_j v_j^2)]+\vec{\nabla}_r[n_j(\epsilon_j+\tfrac{1}{2}m_j v_j^2)]\vec{v}_j+\vec{\nabla}_r(\vec{v}_j\cdot\vec{\vec{P}}_j)-n_j\vec{F}_j\vec{v}_j=-\vec{\nabla}_r\vec{Q}_j+R_2 \tag{4}$$

is the energy transport equation, where ϵ_j is the thermal energy for particles j,

$$R_2=\int\tfrac{1}{2}mw_j^2\left[\frac{\partial f}{\partial t}\right]_{\text{int}}\underline{dw}_j,$$

and

$$\vec{Q}=\frac{m_j}{2}\int(\vec{w}_j-\vec{v}_j)(\vec{w}_j-\vec{v}_j)^2 f\,\underline{dw}_j$$

is the heat flux.

It is obvious that Eqs. (2)—(4) represent the discharge only if it is possible to close the set of equations and to define the force F (that is to say the electric field) and the

interaction terms $S_{j\infty},R_1,R_2$. So it is clear that a macroscopic description of the discharge is necessarily linked to an *a priori* description of the microscopic behavior of the particles inside the collective phenomena.

Fundamental hypothesis

We assume that the propagation of an ionizing wave under an electric field strength, in the experimental conditions hereafter simulated (Wagner[13]), depends on the weakly ionized gas theory. In this context, the electron cloud evolution, considered as a fluid through the neutral gas, is achieved assuming that the neutral gas remains static and uniform and is not heated by the crossing of the ionizing wave which is too fast to disturb the neutral gas.

The interactions between electrons, ions, and excited species can be neglected in regard to the binary collisions between these particles and the neutral particles. Therefore, the interaction term $(\partial f/\partial t)_{\text{int}}$ of Eq. (1) is the rate of change of the distribution function due only to the binary collisions.

The collisional terms $S_{j\infty},R_1,R_2$ of the set of equations depend on the distribution function. We have made the traditional assumption of fluid models, that the energy distribution of electrons in a gas submitted to an electric field is approximatively Maxwellian (Von Engel[14]). This formulation properly represents the experimental static ionization coefficient (Abbas and Bayle[10(a)]). This hypothesis of isotropy of the distribution function results in closure of the system of the equations (2)—(4) if P_e and Q_e are defined by

$$\overleftrightarrow{\mathbf{P}}_e = n_e k T_e \overleftrightarrow{\mathbf{I}} , \tag{5}$$

$$Q_e = 0 . \tag{6}$$

These equations express the assumption that the kinetic pressure tensor is reduced to its diagonal elements and that the electron heat flux is equal to zero. Other formulas for the distribution function could be used, for example, those proposed by Maurel, Bayle, Bayle, and Forn,[15] but their uses would increase the computer time without any decisive improvement owing to the range of E/N values used.

We assume that the positive ions, whose mobility is 2 orders lower than that of the electrons, can be considered as immobile compared to the ionizing wave speed. This hypothesis, without any restrictive nature, is of great interest as it perceptibly reduced the computer time without affecting the accuracy of the results. The equality between the molecule and ion mass leads to instant and complete energy transfers from one species to another. Thus, the ions can be considered in equilibrium with the electric field with a temperature nearly equal to that of the molecules.

In the experimental conditions hereafter simulated (fast electronic shock wave through nitrogen at 200 Torr), the photoionization in the gas remains negligible (Abbas and Bayle[10]).

B. Formulation of the interaction operators

The equations of hydrodynamics in the weakly ionized gas theory allow us to simulate the discharge only if the operators $S_{j\infty},R_1,R_2$ appearing in the equations can be defined. To be completely accurate, the expression of these operators is based on a precise knowledge of the distribution function of the electronic speeds. It is obvious that a hydrodynamic model does not offer knowledge of this distribution function; therefore we use the hypothesis of a Maxwellian distribution function characterized by a temperature being a function of time (this is the dynamic electron temperature). We assume that the operators $S_{j\infty},R_1,R_2$ have the same formal dependence on the dynamic temperature as on the static equilibrium temperature. The equilibrium state is that of a stationary and uniform Townsend discharge with electrons in equilibrium with the electric field, and the mean electron temperature (the characteristic energy) only depends on the value of this electric field. Thus the static electron temperature is only a function of the reduced electric field:

$$T_{es} = f\left[\frac{E_s}{N}\right] \tag{7}$$

or

$$E_s/N = \psi(T_{es}) . \tag{8}$$

The experimental determination of this relationship is based on a measurement of the ratio D_T/μ of the diffusion coefficient to the electron mobility in a quasiequilibrium state mixed with the equilibrium state already defined. The ratio D_T/μ, a function of E_s/N, is directly linked to the mean electron energy, called the characteristic energy ϵ_k. Frost and Phelps[16] showed that the characteristic energy is proportional to the mean thermal energy

$$\epsilon_k = \frac{1}{G}\frac{3}{2}kT_{es} . \tag{9}$$

The factor G depends only on the chosen distribution function. If the distribution is Maxwellian as it has been chosen here G is equal to $\frac{3}{2}$ and so the Einstein relation is found:

$$T_{es}(E/N) = \frac{D_T(E_s/N)}{\mu(E_s/N)} \tag{10}$$

with T_{es} in eV. The relationships between the temperature T_{es} and E_s/N and those between the drift velocity v_d and E_s/N are reported in Sec. II E.

1. *Interaction operator of the densities transport equation*

The source term $S_{e\infty}$ [Eq. (2)] represents the number of ion-electron pairs created per second and per volume unit by the ionizing electron collisions. It is expressed as

$$S_{e\infty}(T_e,n_e,N) = N n_e \int_0^\infty \sigma_i(\epsilon) w(\epsilon) f(\epsilon) d\epsilon , \tag{11}$$

where N is the neutral gas density, and $\sigma_i(\epsilon)$ is the electron-molecule ionizing cross section. A fit of the experimental data from Rapp and Englander[17] gives

$$\sigma_i(\epsilon) = C_i \times 10^{-16}(\epsilon - W_\infty)\Delta(\epsilon - W_\infty) . \tag{12}$$

W_∞ is the ionization energy of the molecule, $W_\infty = 15.6$ eV, $C_i = 3.333 \times 10^{-2}$ cm^2 eV^{-1} for nitrogen. $\sigma_i(\epsilon)$ is then in cm^2. Moreover, the Maxwellian distribution of

the electron gas allows us to give explicit form to Eq. (11) whose resolution leads to

$$S_{e\infty}(T_e,n_e,N)=1.68\times10^{-11}n_eN \times T_e\exp\left[-\frac{W_\infty}{T_e}\right]\left[1+\frac{2T_e}{W_\infty}\right] . \quad (13)$$

This gives the dependence of the collision electron source term with the electronic temperature.

2. *Interaction operator of the momentum equation*

The collisions between electrons and neutral particles are considered as the main disturbance of the electron momentum (Lorentz gas approximation) and the interaction operator is

$$R_1=-n_em_eU_e\nu_e . \quad (14)$$

ν_e is the momentum transfer frequency or elastic collision frequency.

3. *Interaction operator of the energy equation*

Following Abbas and Bayle,[10] the energy initially provided by the electric field at the head of the ionizing wave is dispersed as

(a) ionization energy,

(b) elastic collisions with the neutral particles,

(c) inelastic collisions with the neutral particles (excitation processes),

(d) electron heating.

The accurate determination of each energy loss is a problem dependent on a microscopic analysis. In a macroscopic model, these different processes can simply be estimated, either globally or in individual cases.

(a) In the equilibrium case (stationary and uniform discharge) the energy provided by the electric field is exactly equal to the losses and the energy equation is reduced to

$$n_eE_sv_d=\tfrac{3}{2}T_{es}S_\infty+(\nabla_e+\nabla_i)(\tfrac{1}{2}mw_e^2) , \quad (15)$$

where ∇_e and ∇_i are the symbolic representation of the interaction operators. The electronic velocity is reduced to the drift velocity. The energy lost by electrons is equal to the product E_sv_d that is only a function of the electric field in an equilibrium state. To obtain this product as a function of the static equilibrium temperature, it is necessary to determine the relations

$$T_{es}=f(E_s) \text{ or } E_s=\Psi(T_{es}) . \quad (16)$$

It results from this that in an equilibrium case the energy losses can be expressed either as a function of the electric field by the relation $n_eE_sv_d(E_s)$ or as a function of the static electron temperature alone substituting E_s by its function of T_{es}:

$$\sum(\text{losses})=n_e\Psi(T_{es})v_d(\Psi(T_{es})) =n_e\Phi(T_{es}) . \quad (17)$$

(b) In a nonequilibrium case (nonuniform and transitory discharges), it is no longer possible to fix the losses as a function of the electric field but it is necessary to resort to the dynamic electron temperature T_{ed}, (that is to say, to the value of T_{ed} deduced from the energy equation). If it is assumed that the effect of the expected change in the energy distribution function on the collision interaction term is negligible (this hypothesis introduces no restriction on the losses processes), the formal dependence of the energy losses as a function of the temperature obtained in the equilibrium case [Eq. (17)] can be extrapolated to the nonequilibrium dynamic case. Thus

$$\sum(\text{losses})=n_e\Phi(T_{ed}) . \quad (18)$$

In the function Φ, T_{es} has been replaced by T_{ed}.

C. Practical formalism

This nonequilibrium model, previously described, is applied to the propagation study of the leading edge of an ionizing wave appearing in the breakdown of a plane parallel gap in an impulsed overvoltage. Because of computer time restriction, the formalism is one dimensional. Nevertheless, the three-dimensional behavior of the discharge has been taken into account as seen below. So the model consists of the electron density transport equation

$$\frac{\partial n_e}{\partial t}+\frac{\partial n_eU_e}{\partial x}=S_{e\infty} , \quad (19)$$

the ion density transport equation

$$\frac{\partial n_i}{\partial t}=S_{e\infty} , \quad (20)$$

and the electron momentum transport equation

$$n_eU_e=\frac{n_eq_eE}{m_e\nu_e}-\frac{q_e}{m_e\nu_e}\frac{\partial(n_eT_e)}{\partial x}$$

or

$$n_eU_e=n_ev_d\left[1-\frac{1}{n_eE}\frac{\partial(n_eT_e)}{\partial x}\right] . \quad (21)$$

The mean velocity of the electron gas results from the action of the applied electric field [first term of the right-hand side (rhs)] and from the action of global diffusion phenomena (second term of rhs) [Eq. (21)]. Finally, the electron energy transport equation giving the nonequilibrium temperature is

$$\frac{3}{2}\left[\frac{\partial T_e}{\partial t}+U_e\frac{\partial T_e}{\partial x}\right]=-\frac{1}{n_e}\frac{\partial(n_eT_eU_e)}{\partial x}-\Phi(T_e)+EU_e . \quad (22)$$

We proceed as follows. At an instant t, the electronic densities $n_e(t)$, the ionic densities $n_i(t)$, and the electron temperature $T_e(t)$ are supposed known; the electric field is calculated by the method described in Sec. III and the resulting electron velocity (drift velocity plus thermal velocity) is obtained by means of Eq. (21). The system is then numerically solved by the method of characteristics in an iterative way. This method is applied to find the solution for densities and electronic temperature after a time step

Δt assuming that E, U_e are unchanged during Δt, then we use the new values of n_e, n_i, T_e to find better approximation for E, U_e at $t+\Delta t$. This process of iterations is repeated until the solution of n_e, n_i, T_e converges within a permissible error. These values of n_e, n_i, T_e are then used as the initial condition for a further step.

D. Equilibrium model

To show obviously the role of nonequilibrium between the electrons and the field appearing in the electron shock-wave structure and thus the role played by hot electrons ahead of the discharge, a parallel is made between the results obtained from a second-order model (nonequilibrium model) and those obtained from a first-order model involving an equilibrium state between the electrons and the electric field.

This first-order model is based on the equations of transport of electron (19) and ionic (20) densities and of electron momentum transport (21). As this is an equilibrium situation, the electron temperature is defined by the characteristic energy and is only a function of the reduced electric field defined in Eq. (10).

The source term S_∞ in the electron density equation keeps the same connection with the temperature [Eq. (13)] as for the nonequilibrium model.

In the equilibrium state the source term S_∞ can be identified to the first Townsend coefficient experimentally measured

$$S_{e\infty}(T_{es}, n_e, N) = \frac{\alpha}{N}(E_s/N) N n_e v_d \ . \tag{23}$$

In this relation T_{es} and E_s are linked by relations (24) and the drift velocity v_d is calculated by relations (25). In this case we verified that this source term is perfectly equal to the experimental data of $\alpha(E/N)/N$ given by Dutton.[18]

E. Relationships at the equilibrium case between the reduced field E_s/N and the static electronic temperature and between the reduced field E_s/N and the drift velocity v_d

The relationships used in Ref. 10 have been slightly modified to obtain a best fit of the source term S_∞, of the drift velocity v_d and of the static temperature T_{es} on the experimental results. In the case of the drift velocity and of the characteristic energy, the former relations available for the whole range of variation of the electric field have been replaced by a set of formulations, each one of these relations being adapted to a part of the variation of the electric field or of the electron temperature. This is of great interest because of the wide range of variation of these two parameters on the front of the ionizing wave and because of the excessive sensitivity of the calculation linked to the twice-exponential variation of the densities with the electron temperature.

The experimental works of Kontoleon, Lucas, and Virr[19] for values of E_s/N between 130 and 850 Td and those of Naidu and Prasad[20] for E/N below 130 Td give D_T/μ as a function of E_s/N. The relation $T_{es}=f(E_s/N)$ is obtained by means of a least-mean-squares fit from these works.

The expression of T_{es} (eV) has been obtained in the following form:

$$T_{es} = a + b\left[\frac{E_s}{N}\right] + c\left[\frac{E_s}{N}\right]^2 , \tag{24}$$

T_{es} in eV and E_s/N in Td. The values of coefficients a, b, and c are different for the different range of E_s/N (Td) and are reported in Table I.

In recent experimental works, Flechter and Reid[21] measured the drift velocity v_d of electrons in nitrogen for a large range of applied electric fields ($57 \le E_s/N \le 567$ Td). The formulation of the relations of dependence of the drift velocity function of the reduced applied field is taken from these results. For higher values of E_s/N, the experimental results of Schlumbohm[22] show a slower increase of the drift velocity with E_s/N. The least-mean-squares fit applied to these results gives the following relations. For $E_s/N \ge 334$ Td,

$$V_d = 2.58\times 10^7 \ln\left[\frac{E_s}{N}\right] - 1.2\times 10^8 \ .$$

For $9.1 \le E_s/N \le 334$ Td,

$$V_d = 3\times 10^6 + 8.04\times 10^4 (E_s/N) \ . \tag{25}$$

For $E_s/N \le 9.1$ Td,

$$V_d = 4.21\times 10^5 (E_s/N) \ .$$

V_d is in cm s^{-1} and E_s/N in Td.

III. CALCULATION OF THE SPACE-CHARGE ELECTRIC FIELD

A. Expression of the electric field

In order to be applied, the earlier hydrodynamic model needs the addition of the equation governing the space-charge electric field. It is well known (Wagner[13]) that the electron avalanche, issuing from a group of primary electrons released by the cathode, evolves first as a sphere

TABLE I. Coefficients a,b,c for different ranges of E_s/N used in Eq. (24).

E_s/N (Td)	$\frac{E_s}{N} < 97.09$	$97.09 < \frac{E_s}{N} < 303$	$303 < \frac{E_s}{N} < 1210$	$\frac{E_s}{N} > 1210$
a	9.02×10^{-1}	-1.18×10^{-1}	8.07×10^{-1}	6.14
b	1.13×10^{-2}	1.96×10^{-2}	1.36×10^{-2}	4.72×10^{-3}
c	-3.7×10^{-5}	-1.37×10^{-5}	-4.08×10^{-6}	0

whose radius is equal to the electron diffusion radius; then, as the carrier number increases the collective phenomena of carrier interaction applies in two ways.

(a) An electrostatic mode, by means of a change of the value of the electric field strength and of its force lines.

(b) An energetic mode, discussed later but showing a longitudinal diffusion, much higher than the transverse diffusion. The rhs of Eq. (21) gives a representation of this fact.

Both these phenomena give a high anisotropy of the electron cloud which tends to lengthen in the direction of the electric field. The discharge evolves in a filamentary stage and its radial extension is lower than its longitudinal one. It appears that the monodimensional Poisson equation is coherent with the formalism and we presented it in a previous paper.[10] This involves, however the assumption the charges are spread in infinite planes perpendicular to the propagation axis. This may lead to an overestimation of the electric field. To avoid this drawback, Davies and Evans[23] calculated the space-charge field, assuming that the charge carriers are in a cylinder with a flat end. Its radius is equal to the electron diffusion radius. They assumed that the charges and the field are constant on a cross section and equal to their axial values. The resulting field is obtained by the superimposition of the elementary fields created by all the discs uniformly charged and placed at the network points of the gap. When the discharge propagates, the cylinder lengthens without modifying its radius or its bottom form. This analysis has been carried on (Caumes,[24] and Bayle, Bayle, and Caumes[25]) with the following different assumption: The charges are supposed to be distributed inside elementary cylinders of thickness equal to the network mesh and the net space-charge density inside an elementary cylinder is assumed to be constant. The total field created at a point of the discharge is the result of the superimposition of the elementary field ΔE of each cylinder. This method can be called the "constant net space-charge density cylinder method" (CNC). The accuracy of the calculation can be improved, assuming that the net space-charge density evolves linearly inside an elementary cylinder and this method can be called the "variable net space-charge density cylinder method" (VNC).

B. Study of the profile of the discharge front

The previous computations are based on the hypothesis that the discharge evolves in a cylinder with a flat end and propagates without deformation. In fact, the space charge induced by the electrons and the ions yields not only a change in the resulting field strength, but also a change in the form of the lines of field. However, the revolution symmetry around the propagation axis is maintained. This induces an anisotropy of the transport and diffusion phenomena, leading to the conclusion that the tip of the discharge channel cannot end on a plane surface.

To study the influence of the modification of the lines of force on the profile of the discharge channel, we first suppose that the charges $n_e(x,t)$ and $n_i(x,t)$ defined by relations (28) are distributed inside a flat-ended cylinder with a radius $R_D=0.15$ cm. This constitutes the situation in the first-order model described in Ref. 5. The value of 0.15 cm for the cylinder radius is the radius of the channel estimated from Wagner experiments[13] and used by Davies[1] and Abbas and Bayle[5] to define the discharge channel.

From this cylindrical repartition, the lines of force are calculated by numerically resolving the Poisson equation:

$$\frac{\partial^2 V}{\partial x^2}+\frac{1}{r}\frac{\partial V}{\partial r}+\frac{\partial^2 V}{\partial r^2}+\frac{\rho(x,r)}{\epsilon_0}=0\,. \tag{26}$$

The question was whether the lines of force were sufficiently perturbed to modify the flat end of the cylinder. It is indeed what we noticed. A convergence of the lines of force occurs, just ahead of the discharge channel (Fig. 1). This convergence takes place in the zone where the electron density is about 3 orders lower than the higher density of 4×10^{-7} C/cm^3. This modification of the lines of force, parallel at the origin, yields a charge confining and thus a narrowing of the envelope of the discharge, ahead of the wave. In consequence, the propagation of the wave front cannot be developed on the cross section of a cylinder whose radius remains constant all over its length. It is necessary to define a profile for the discharge front that is able to produce an electrostatic confining (leading to a tip effect) and show the effect of the electron pressure gradient (leading to a modification of the longitudinal diffusion).

The most suitable profile for these constraints seems to be ellipsoidal, maintaining axial symmetry and lengthening in the direction of propagation. A similar profile of the discharge channel has been set up by Lozansky and Firsov[26] with the assumption that the channel was perfectly conducting and that the tip of the ellipsoid had a constant curvature radius, whereas in this work we consider a variable curvature radius for the tip of the ellipsoid.

In the transverse direction, the small axis of the ellipsoid is chosen equal to the radius of the transverse electron diffusion R_D, which is experimentally measured. The radial extension of the discharge and particularly the extension radius of the channel appearing behind the ion-

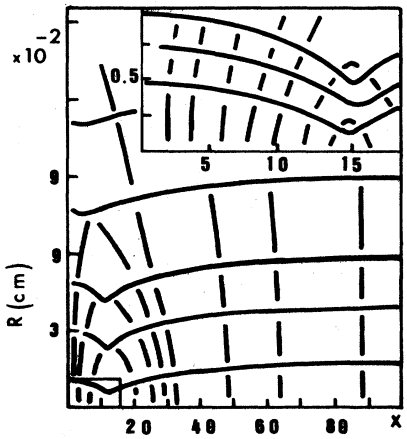

FIG. 1. Equipotential lines (dashed lines) and lines of field (solid lines) corresponding to the initial net space-charge density. Each tic on the x axis is equal to 6.533×10^{-3} cm.

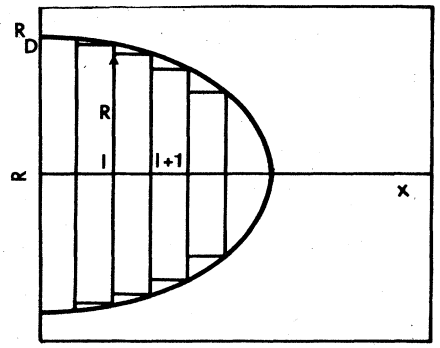

FIG. 2. Ellipsoidal envelope of the discharge.

izing wave front, i.e., between the cathode and the wave front, is established by this parameter. In this part of the discharge, the radius remains nearly constant and the net space-charge density is low. It is a glow discharge-like situation with a low field (Abbas and Bayle,[5] and Davies and Evans[23]). The long axis choice is more difficult. We define this ellipsoid by the focusing of the electron cloud under the effect of the lines of force. To show the role of localization of the charges, we assume that the ratio of the highest density (at the limit of the channel) to the lowest density (just ahead of the front) equal to 10^3 defines the envelope of the useful part of the electron cloud in the field computation. The focusing of the lines of force of the electric field nearly occurs at this point. We verify by the tests carried out that the electronic densities situated outside of the envelope, which are not taken into account in the field calculation, intervene in a negligible way in this field value. We found that the definition of the envelope at 10^3 was a good choice as it is able to show the convergence of the lines of force ahead of the channel without introducing notable changes in the field calculation. The electron cloud is inside this ellipsoidal envelope and for the field calculation only we consider that there are no electrons in the area outside the envelope. The field computation is carried out by one of the two previously described methods (CCN or CVN). The ellipsoid is cut in elementary cylinders of variable radius (Fig. 2), each section radius being equal to

$$R_x = R_D \left[1 - \frac{x^2}{x_T^2}\right]^{1/2} \tag{27}$$

(x_T being the abscissa of the ellipsoid tip).

It is necessary to elucidate if, during the spatial evolution of the discharge, the radius of curvature of the ellipsoid at its tip evolves. We allow the profile of the ellipsoid to vary during the propagation, by a variation of its long axis and a change in its curvature radius at the tip. During the spatiotemporal evolution of the discharge, the ellipsoid modification follows the evolution of the electron density. This limit of the plasma propagates locally (near the axial tip) like a one-dimensional plane wave. The modification of the ellipsoid gives rise to a cylinder of constant radius R_D behind the front as found in Eq. (27). This new definition of the discharge front plays a determinative role in the electric field configuration.

Figure 3 gives a comparison between two calculations

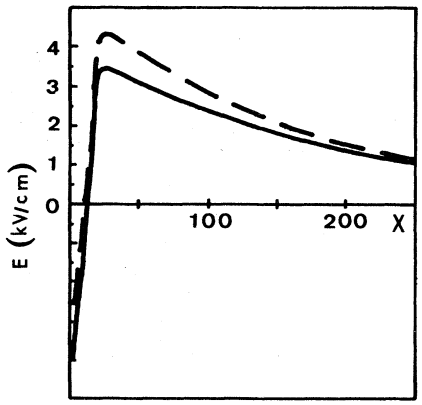

FIG. 3. Comparison in the electric field calculated by the cylindrical model (solid line) and the ellipsoidal model (dashed line) applied to the initial net space-charge density defined in Fig. 5.

of the electric field due to the charge carriers situated in the analysis window

(a) assuming the envelope is a cylinder with a flat end (solid line),

(b) assuming the envelope is the ellipsoidal model above defined (dashed line).

In the two calculations, the charges repartition $n_e(x)$ and $n_i(x)$, have the same value, and are those defined in Sec. IV A [Eq. (28)]. The ellipsoidal envelope shows a tip ef-

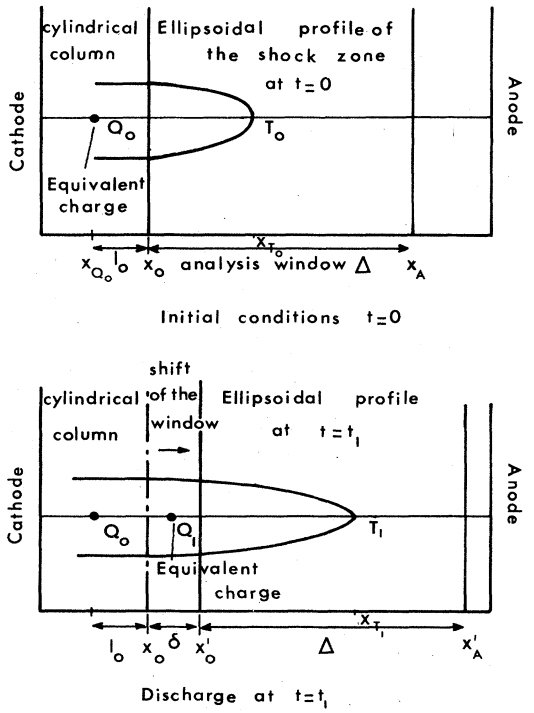

FIG. 4. Definition of the analysis window. T_0 and T_1 are defined by the ratio $n_e(\max)/n_e(x_T) = 10^{-3}$ and fix the tip of the ellipsoid used for the field calculation.

fect characterized by an increase in the maximum value and the field gradient ahead of the front. This tip effect will give an enhancement of the shock and a higher degree of localization of the electrostatic phenomena.

IV. PROPAGATION OF ELECTRON FLUID WAVE

A. Description of the simulated experimental work. Initial and boundary conditions

We studied the propagation of a ionizing wave in a breakdown in nitrogen in a 3-cm plane-parallel gap. The applied electric field was equal to 10.6 $kV\,cm^{-1}$ and the gas pressure (nitrogen) was equal to 200 Torr, leading to an overvoltage of about 25%. These experimental conditions were those of Wagner's[13] experiment. This experimental situation has been analyzed by one of us in previous works (Abbas and Bayle[5,10]). The simulation of the discharge by a first-order model shows that the discharge front evolves in an unavoidable way towards the formation of an electron shock wave, whose propagation will be studied. The shock conditions obtained 125 ns after the release at the cathode of the initiating electrons are the initial conditions in this work.

For the computer analysis, it was necessary to treat only a part of the gap and this involved the definition of an analysis window, situated in front of the discharge. It corresponded to the front of the anode-directed streamer and held the electron shock wave (Fig. 4). The length of the studied area measured 0.163 cm and was divided in 250 meshes. The spatial resolution was $\Delta x=6.53\times10^{-4}$ cm and the temporal resolution was $\Delta t=3\times10^{-12}$ s. The initial conditions for the ion and electron densities, the electric field, and the electron temperature are shown in Figure 5(a). Towards the left of the analysis window, the discharge is a quasipositive column with nearly equal ion and electron densities with cold electrons in a weak electric field. On the right-hand side, few hot electrons evolve in a strong field. The initial profiles of the ion and electron densities are identified as exponentially decreasing curves, based on the previous works (Abbas and Bayle[5]). For $x \le x_c$

$$n_e(x,0)=n_{e0}\,,$$

$$n_i(x,0)=n_{i0}\,,$$

and for $x > x_c$ (28)

$$n_e(x,0)=n_{e0}\exp[-k_e(x-x_c)]\,,$$

$$n_i(x,0)=n_{i0}\exp[-k_i(x-x_c)]\,,$$

with $n_{e0}=4\times10^{-7}$ $C\,cm^{-3}$ and $n_{i0}=3.5\times10^{-7}$ $C\,cm^{-3}$. The shock is defined as the narrow transition zone between a region of the gas with high charge-carrier densities and a region without charge carriers. The values of coefficients k_e and k_i represent the electron shock-wave strength:

$$k_i=1500\,,$$

(29)

$$k_e=1000\left[1-\frac{x-x_c}{x_L-x_c}\right],$$

with $x_L=(x_0+x_A)/2$,

$$n_e(x,0)=n_i(x,0)=0 \quad \text{for } x > x_L$$

where x_0 is the initial left boundary of the analysis window and x_A is the window boundary towards the anode. x_c is the point from which the electronic and ionic densities begin to decrease (see Fig. 4). During the spatio-temporal evolution of the discharge, the relative gradient k_e of the electron density represents the shock-wave strength. The left and right boundaries of the window are far enough removed from the electrodes for the virtual charges, carried by the metallic electrodes, to be ignored.

It is obvious that all the charges taken into account in the analysis window do not constitute an isolated system and this implies the necessity of determining the interaction of the whole discharge with the studied area. This action is the result, on the left-hand side of the investigated zone, of the closeness of charge carriers of the discharge channel and appears as an electrostatic effect.

The charge repartition is then as follows: As a further approximation, the charge in the cylindrical column for $x < x_0$ is replaced by a charge Q_0 located at a position $x_{Q_0}=x_0-l_0$ from the cathode. This position is the center of gravity for the electron and ion cloud and is estimated from the results of the first-order model (Abbas and Bayle[5]). This part of the discharge creates an electric field

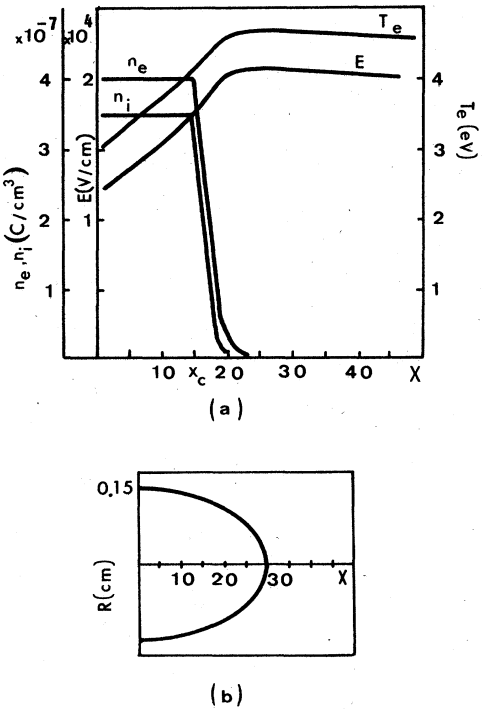

FIG. 5. Initial conditions at $t=0$ [corresponding to $t=125$ ns from Abbas and Bayle (Ref. 5)]. (a) Initial electron density n_e, ion density n_i, electric field E, and electron temperature T_e. (b) Initial ellipsoidal envelope. Each tic on the x axis is equal to 3.266×10^{-3} cm.

equal to 6 kV/cm on x_0, the initial left boundary of the analysis window.

In the analysis window, the charges are distributed inside the ellipsoidal envelope and, only in the electric field computation, we consider there are no electrons outside. The initial electric field $E(x,0)$ in the analysis window is equal to the sum of the applied field E_A plus the field $E(Q_0)$ created by the charge Q_0 plus the field $E(W)$ created by the charges located inside the ellipsoid:

$$E(x,0)=E_A+E(Q_0)+E(W) . \tag{30}$$

$E(W)$ is calculated assuming that the charges distribution in the ellipsoidal envelope are represented by a set of disks (as shown in Fig. 2) within which the charge density is assumed constant at the value calculated for the value of x appropriate to the disk.

Once the analysis window is clearly defined the evolution of the ionizing wave must be allowed to occur while preventing it from reaching the right boundary of the window. It should be borne in mind that this event will introduce the problem of electron cloud impact with an absorbing wall. To avoid this drawback, the window was shifted with time towards the anode, the total shift being equal to 0.294 cm in 2.4 ns. Each shift was carried out in such a way that only the left part of the positive glowlike column was affected by the boundary shift. The charges remaining on the left of the analysis window were taken into account by the electric field they created in the window. The fact that the zone of the quasi positive glowlike column is a cold area with a weak net space-charge density of generation and transport rates nearly equal to zero justifies this procedure. The electric field at the time t is then the sum of $E(Q_0)$ plus E_A plus $E(Q_1)$, the field created by the charges left by the window shift plus $E(W)$. Therefore

$$E(x,t)=E_A+E(Q_0)+E(Q_1)+E(W) . \tag{31}$$

The electron temperature T_e is initially supposed to be an equilibrium temperature as defined in relation (24).

In the following figures, the abscissa origin is the x_0 position of the left boundary of the window as has been defined according to the initial conditions. The integer values on the abscissa axis are values of the factor M by which Δx must be multiplied in order to obtain the position of the point by reference to the position x_0 of the initial conditions ($\Delta x = 6.53\times 10^{-4}$ cm).

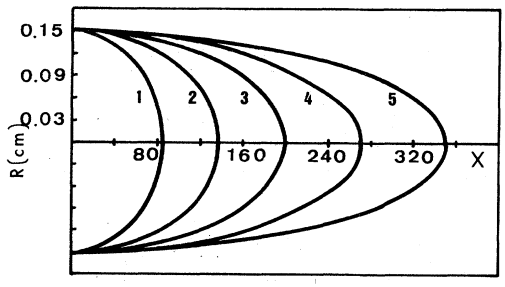

FIG. 6. Deformation of the discharge envelope during the temporal evolution. $t_1=0.6$, $t_2=1.05$, $t_3=1.5$, $t_4=1.95$, $t_5=2.4$ ns. Each tic on the x axis is equal to 0.0261 cm.

B. Results and discussion

1. General description of the propagation mechanism

The evolution of the discharge envelope points out in a general way the channel propagation in the neutral gas. Figure 6 shows the progressive change in the ellipsoid pattern, when the transverse diffusion radius of the quasi positive glowlike column is kept constant and equal to its experimental data. We assume this radius is nearly constant in the positive glowlike column (the ambipolar diffusion is slow enough so that the column radius does not change). One may notice that the channel is progressively accelerated and that the ellipsoid profile is modified. The long axis is lengthened in the propagation direction and the curvature radius at its end rapidly decreases, yielding a tip effect. This fact is of great significance to the discharge evolution as the electric field ahead of the front is greatly amplified as shown in Fig. 7. These increasingly high-field values are at the same time more and more located in front of the channel, the tip effect leading directly to an increase in the electron drift. Figure 8 shows the simultaneous evolutions of the ion and electron densities and of the dynamic electron temperature [deduced from Eq. (22)] and of the electric field. One may notice that the low electron temperature in the positive glowlike discharge keeps the densities varying slowly with time. The net space-charge density remains nearly constant in this part of the discharge and evolves towards a quasineutrality in this part of low electron temperature and weak electric field. On the opposite side, in the shock area ahead of the channel the electron temperature is high. The largest part of the electron production takes place in this zone because of this temperature increase, and this induced here a strong ionization rate. The net space-charge density, nearly constant in the column, greatly increases in the shock-wave front. This implies a parallel increase of the resulting field. Hence an amplification process develops, the increase in the field strength leading to an increase in the speed of the electrons ahead of the cloud. This implies a partition of the carriers in the front, the ions remaining quite immobile. So a progressive deformation appears on the ellipsoid pattern with

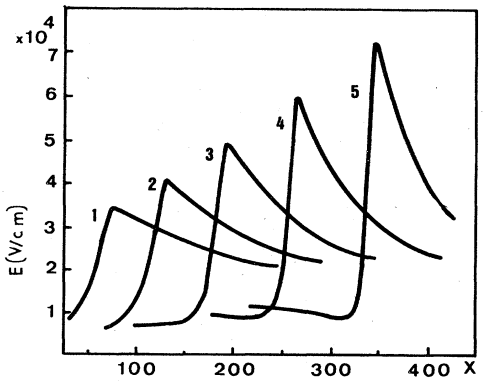

FIG. 7. Spatio-temporal evolution of the electric field. $t_1=0.6$, $t_2=1.05$, $t_2=1.5$, $t_4=1.95$, $t_5=2.4$ ns. Each tic on x axis is equal to 0.0326 cm.

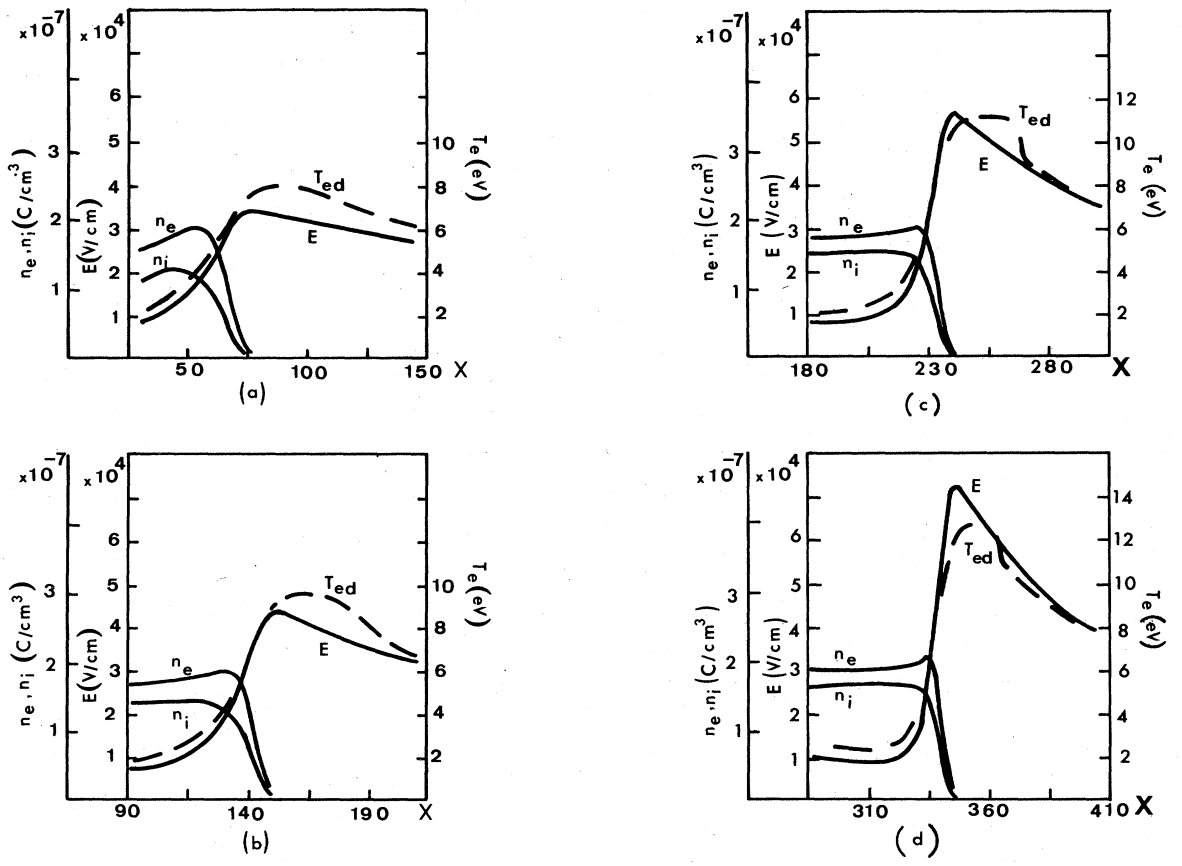

FIG. 8. Evolution of the profile of electron and ion densities, electric field, and electron temperature vs time. Each tic on x axis is equal to 0.0163 cm. (a) $t=0.6$ ns, (b) $t=1.2$ ns, (c) $t=1.8$ ns, (d) $t=2.4$ ns.

an increase of the tip effect by a decrease of the curvature radius of the end of the ellipsoid. This phenomenon is greatly emphasized by the high degree of localization of the field maximum ahead of the ionizing front. Only electrons present in this zone are affected by this increase. This localization of the field effect is correlated with an enhancement of the heating effect of electrons. The result is to maintain and even reinforce the shock-wave structure in the front of the ionizing wave.

The electron temperature, among the parameter values, evolves the more rapidly, particularly just in the shock zone. The temperature curves show that one of the first phenomena of the propagation is the importance of the strong heating of electrons that takes place on the wave front. Equation (13), giving the expression of the source term of ionization, shows that this temperature rise induces an electron overproduction that, simultaneous with the acceleration due to the tip effect, leads to an acceleration of the propagation. Hence the high-speed propagation arises from the double contribution of local perturbations coming from electrostatic phenomena (increase of the drift velocity on the wave front) and from energetic phenomena (overproduction of hot electrons). After an acceleration phase, the wave velocity reaches a nearly constant value of 1.2×10^8 cm/s, in perfect agreement with experimental data of Wagner.[13]

2. *Permanence of the electron shock wave during the wave propagation*

It is necessary to clarify whether the electron shock-wave maintains itself and/or is amplified during the propagation. In a general way, the spatio-temporal variation of the different values (Figs. 8—10) show the permanence

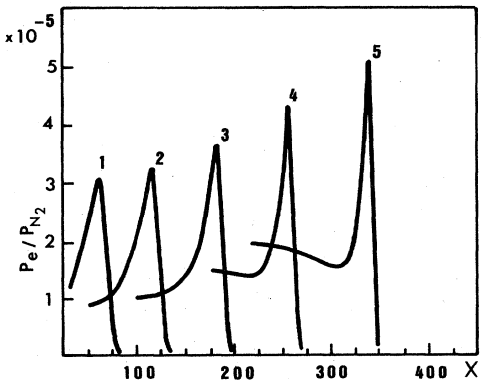

FIG. 9. Spatio-thermal evolution of the ratio of the electron pressure P_e on the neutral pressure P_{N_2}. $t_1=0.6$, $t_2=1.05$, $t_3=1.5$, $t_4=1.95$, $t_5=2.4$ ns. Each tic on the x axis is equal to $x=0.0163$ cm.

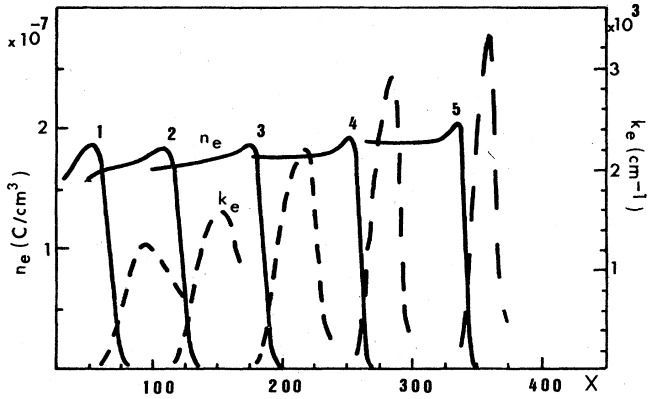

FIG. 10. Electronic densities and relative gradients. $t_1=0.6$, $t_2=1.05$, $t_3=1.5$, $t_4=1.95$, $t_5=2.4$ ns. Each tic on the x axis is equal to 0.0163 cm.

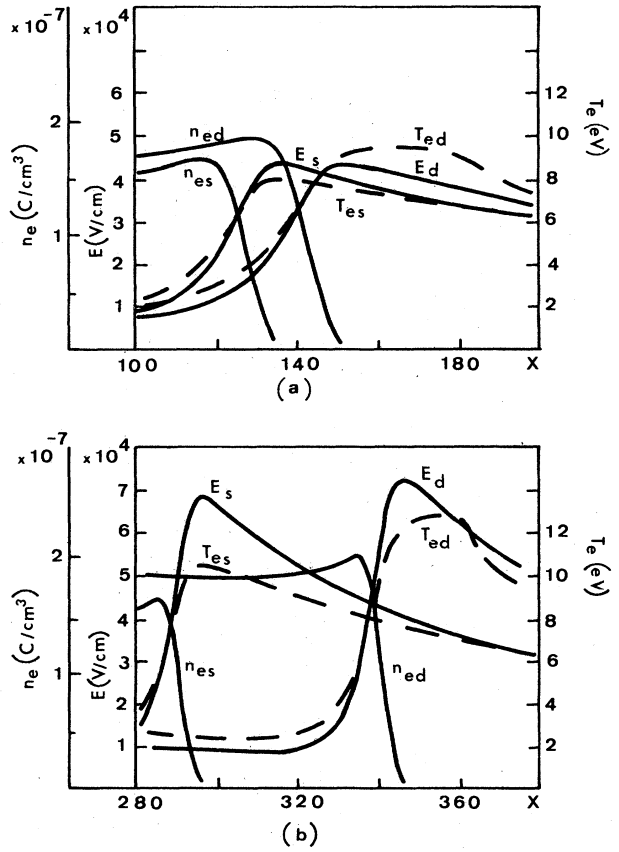

FIG. 11. Comparison between the nonequilibrium field E_d and the equilibrium one E_s, the dynamic nonequilibrium temperature T_{ed} and the static equilibrium temperature T_{es}, and the nonequilibrium electronic densities n_{ed} and the equilibrium densities n_{es}. Each tic on the x axis is equal to 0.0131 cm. (a) $t=1.2$ ns, (b) $t=2.4$ ns.

and enhancement of the electron shock wave by a maxima increase and a half-width decrease. The evolution of these variables is perfectly represented by the evolution of the ratio of the electron pressure P_e to the neutral pressure P_{N_2} (Fig. 9). The electron pressure P_e represents the electron energy density and in a previous paper (Abbas and Bayle[10(b)]) we have shown the decisive role played by P_e. The evolution of the electron pressure $P_e=n_e kT_e$ appears as the result of the conjugate electrostatic and energetic effects. It is the value that best reproduces the evolution of the discharge front. Figure 9 allows us to draw conclusions about the permanence and amplification of the electron shock-wave structure, which appears to drive the ionizing wave. The relative gradient of electron densities $k_e=(1/n_e)(\partial n_e/\partial_x)$ represents the shock-wave strength and reaches high values ahead of the electron density maximum. In this zone there is the greatest number of hot electrons in nonequilibrium with the electric field, having a higher temperature than the temperature deduced from Eq. (24) (Fig. 10).

3. *Role of hot electrons in the propagation*

After the study of the mechanisms of propagation of the electron shock wave and its permanence during the propagation, the reasons of the propagation need to be analyzed. The intricacy of the involved processes linked to the complexity of both the phenomena and the formulation do not allow simple conclusions and it appears illusory when analyzing the collective phenomena to identify what is the cause and what is the effect. To solve this problem, we chose to compare two different models of discharge, involving different formalisms, and to analyze the possible differences appearing between their results.

The first model is the one we developed above. It takes into account the concept of nonequilibrium between electrons and the electric field as introduced by the definition of the electron shock wave. This model is based on Eqs. (19)—(22).

The second model is an equilibrium model. It assumes that the electrons are in equilibrium with the electric field, and their temperature is the static temperature deduced from the characteristic energy. This model is based on Eqs. (19)—(21). The electron static temperature is obtained from the electric field by the relation (24).

Hence, except for the fundamental definition of the electron temperature, this second model is exactly identical to the first, particularly in the formulation of the source term of the transport equation of electron and ion densities. The electric field calculation is made by CNC method, assuming in the two models that the discharge evolves in a ellipsoidal envelope. Of course, the initial conditions are the same in the two models and are those described in Sec. IV A.

Figure 11 shows the evolution of the electron densities, the electric field, and the electron temperature in the two models, 1.2 and 2.4 ns after the initial conditions. The values obtained by the equilibrium model are written with $s(n_{es},T_{es},E_s)$ because it uses the static temperature and the values obtained by the nonequilibrium model are written with $d(n_{ed},T_{ed},E_d)$ because this model uses the dynamic temperature. The curves for the electric fields E_d and E_s show similar variations. It is obvious that the

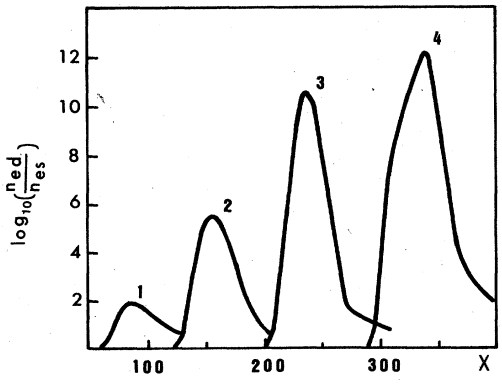

FIG. 12. Ratio of nonequilibrium electronic densities n_{ed} to equilibrium electronic densities n_{es}. Each tic on the x axis is equal to 0.0326 cm. $t_1=0.6$, $t_2=1.2$, $t_3=1.8$, $t_4=2.4$ ns.

relative positions of the maxima cannot concur because the electron generation and thus the spread of the canal are not the same in the two models. However, these curves show that the significance of the electrostatic phenomenon is the same in the two situations. This is linked to the fact that the evolution of the electric field is greatly determined by the net space-charge density change inside the ellipsoid. Notice that the greater the distance between these maxima (i.e., the more the ellipsoids are different), the greater the difference between the values of these maxima. The evolution of the electron temperature depends on the model used. In the equilibrium model, the temperature and the field evolve in the same way and their respective maxima appear at the same place. In the nonequilibrium model, the field and the temperature do not evolve in monotonous ways and the temperature maxima are located in front of the field maxima. Therefore, the role of nonequilibrium effects on the discharge propagation is settled for situations where the significance of the electrostatic phenomena is similar. The space-charge effects leading to a reinforced field in front of the channel are not sufficient to induce over-acceleration. The curves show that the hot electrons induce the overproduction in front of the channel leading to an increased acceleration of the ionizing wave propagation. The relative values of the propagation velocities are, respectively, equal to 8.5×10^7 cm/s in the equilibrium model and 1.2×10^8 cm/s in the nonequilibrium model. This last value agrees with the data obtained by Wagner[13] for the last stage of the anode directed streamer. This electron heating on the wave front creates a precursor effect ahead of the plasma channel while, in the positive glowlike column, the field and temperature values are low enough for the two models to give nearly the same results. This precursor effect generated by the energetic nonequilibrium between the electrons and the electric field is shown in Fig. 12 giving the ratio n_{ed}/n_{es} of the electron densities obtained by each model. Figures 8 and 12 show that the wave front acts like a source of hot electrons, with little spatial extension.

If these results are compared with the results obtained in the analysis of experimental image converter records (Caumes,[23] Bayle, Bayle, and Caumes,[24] and Bayle, Bayle, and Morales[27]), one may notice that in both cases the formation of a strong field gradient with shock-wave effect was observed. However, the over-voltage was not the same in these two studies. The different values used in the experimental works are reported in Table II.

TABLE II. Experimental work data showing the formation of a strong field gradient.

Reference	E/N (Td)	Pressure (Torr)	Mixture
Bayle, Bayle, and Caumes, Ref. 25	409.60	130	90% N_2
Caumes, Ref. 24	409.60	130	10% O_2
Bayle, Bayle, and Morales, Ref. 27	367	130	97.5% N_2 2.5% CH_4

These experimental works involve too-high E/N values and the numerical computer treatment overflows and we choose to simulate Wagner's experiments involving lower values of E/N (159 Td). For high values of E/N, the charge separation is probably increased and this can explain the second field maximum which is not observed in this work.

On the other hand, it is interesting to correlate our results with those obtained in a point-plane gap in air by Hartmann.[28] He deduced the mean value of the electronic temperature in the active front of the discharge from a fine analysis of the emitted spectrum of the streamer tip and he found about 10—15 eV, which completely agrees with our calculated electronic temperatures.

V. CONCLUSION

The analysis of the front of the first ionizing wave by a hydrodynamic second-order model allows us to characterize the precursor effect, set forth in many experimental works. The whole collision-dominated phenomena (electron production, transport, diffusion) gives rise to the formation of an electron shock-wave structure, ahead of the channel. In this zone, because of the strong field gradients, the electrons are no longer in equilibrium with the field and their energy no longer appears as a function of the field alone. This induces a great modification of the elastic and inelastic interactions with the neutral particles, globally taken into account by our model. The electron shock wave appears then as a zone of high electron temperature leading to an increase in the ionizing collisions. The observed overproduction of electrons is the result of nonequilibrium mechanisms between the electrons and the field.

This high overproduction of electrons (linked to an increase of the thermal electron energy) takes place under a strong electric field and constitutes the driving phenomena of the discharge and so the precursor. The agreement with Wagner's experimental data confirms our model, which appears very satisfying in the range studied.

ACKNOWLEDGMENTS

We wish to thank Dr. Bui Ai for supporting and providing facilities for this work.

[1]A. J. Davies, C. S. Davies, and C. J. Evans, Proc. IEEE, **118**, 816 (1971).
[2]L. E. Kline, J. Appl. Phys. **45**, 2046 (1974).
[3]K. Yoshida and H. Tagashira, J. Phys. D **9**, 485 (1976).
[4]P. Bayle and M. Bayle, Z. Phys. **266**, 275 (1974).
[5]I. Abbas and P. Bayle, J. Phys. D **13**, 1955 (1980).
[6]R. G. Fowler and G. A. Shelton, Phys. Fluids **17**, 334 (1974).
[7]E. E. Sanmann and R. G. Fowler, Phys. Fluids **18**, 1433 (1975).
[8]N. W. Albright and D. A. Tidmann, Phys. Fluids **15**, 86 (1972).
[9]R. Klingbeil, D. A. Tidmann, and R. F. Fernsler, Phys. Fluids **15**, 1969 (1972).
[10](a) I. Abbas and P. Bayle, J. Phys. D **14**, 649 (1981); (b) **14**, 661 (1981).
[11]H. Jurenka and E. Barreto, J. Appl. Phys. **53**, 5 (1982); **53**, 3481 (1982).
[12]H. Jurenka, J. Appl. Phys. **53**, 6115 (1982).
[13]K. H. Wagner, Z. Phys. **204**, 177 (1967).
[14]A. Von Engel, *Ionized Gases* (Oxford University, London, 1965).
[15]J. Maurel, P. Bayle, M. Bayle, and G. Forn, *Third International Symposium on Gaseous Dielectrics, Knoxville,* edited by L. G. Christophorou (Pergamon, New York, 1982), p. 45.
[16]L. S. Frost and A. V. Phelps, Phys. Rev. **127**, 1621 (1962).
[17]D. Rapp and P. Englander, J. Phys. Chem. **43**, 1464 (1968).
[18]J. Dutton, J. Phys. Chem. Ref. Data, **4**, 577 (1975).
[19]N. Kontoleon, J. Lucas, and L. E. Virr, J. Phys. D **6**, 1237 (1973).
[20]M. S. Naidu and A. N. Prasad, J. Phys. D **1**, 763 (1968).
[21]J. Flechter and I. D. Reid, J. Phys. D **14**, 2275 (1980).
[22]H. Schlumbohm, Z. Phys. **182**, 317 (1965).
[23]A. J. Davies and C. J. Evans, Proc. IEEE **114**, 1547 (1967).
[24]G. Caumes, Thèse de Doctorat 3ème Cycle No. 2589, Université Paul Sabatier, Toulouse, France, (1982).
[25]P. Bayle, M. Bayle, and G. Caumes, J. Phys. D **16**, 2449 (1983).
[26]E. D. Lozansky and O. B. Firsov, J. Phys. D **6**, 976 (1973).
[27]P. Bayle, M. Bayle, and E. Morales, J. Phys. D **13**, 563 (1980).
[28]G. Hartmann, Thèse de Doctorat d'Etat No. 1783, Université de Paris-Sud, France (1977).